



PIEZOELECTRIC SMART ISOLATION SYSTEM FOR SEISMIC PROTECTION OF PRECISION EQUIPMENT

Lyan-Ywan Lu¹, Ging-Long Lin², Yi-Zhen Chen³ and Jun-Ger Yeah⁴

ABSTRACT

In many high-technology factories, fragile precision equipments may lose their functionality due to a seismic ground motion. Conventional isolation systems may effectively reduce the acceleration response of equipments, but they may also have a large isolator displacement in a near-fault earthquake with long-period pulse or a severe earthquake. In this study, a semi-active isolation system named “Piezoelectric Smart Isolation System (PSIS)” was proposed to enhance the seismic resistance ability of precision equipments. A PSIS system is composed of a sliding isolation system and a piezoelectric friction damper. The clamping force of the piezoelectric friction damper is regulated by a piezoelectric actuator, so the slip force of the damper becomes controllable. Due to its low energy demand and quick response, the piezoelectric actuator is chosen as the control device in this study. Based on experimental data of a piezoelectric actuator, the seismic response of the PSIS was simulated and investigated in this paper. The result showed that in a near-fault earthquake with long-period pulse, the PSIS is able to effectively reduce the equipment acceleration, and at the same time prevent a large isolator displacement that may damage the underlying piping system under the precision equipment. In addition, the control energy demand of the PSIS was also evaluated and compared with that of an isolation system controlled by an active device.

Keywords: base isolation, piezoelectric actuator, semi-active control, friction damper, precision equipment, smart system.

INTRODUCTION

In high-technology factories, precision equipment such as those used for the production of advanced integrated circuits or for precision metrology usually requires environments with extremely low vibration (Ungar et. al., 1990). A high-technology factory may have two major vibration problems. One problem is caused by ambient vibration and the other is due to seismic vibration. Ambient vibration is usually induced by nearby traffic, mechanical vibration or personnel walking in the high-tech factory, whereas the seismic vibration is caused by an earthquake. Compared with ambient vibration, the primary frequency content and the amplitude of the seismic vibration is usually difficult to be predicted. Therefore, in many high-technology factories, fragile precision equipments may lose their functionality in a sever earthquake.

It has been proven that seismic isolation using sliding-type bearings is an effective technology for protecting seismic structures or equipment (Naeim and Kelly, 1999; Yang et. al., 2005; Lu and Yang, 1997). Nevertheless recent studies have revealed that when a conventional isolation system (passive

¹ Professor, Department of Construction Engineering, National Kaohsiung First University of Science and Technology, Kaohsiung, Taiwan. Tel: 07 6011000 ex.2127. Email: lylu@cems.nkfust.edu.tw

² Ph.D. student, Institute of Engineering Science and Technology, National Kaohsiung First University of Science and Technology, Kaohsiung, Taiwan.

³ Graduate student, Department of Construction Engineering, National Kaohsiung First University of Science and Technology, Kaohsiung, Taiwan.

⁴ Undergraduate student, Department of Construction Engineering, National Kaohsiung First University of Science and Technology, Kaohsiung, Taiwan.

isolation system) with a constant frequency is subjected to a near-fault earthquake (Loh, 1999), which usually possesses a long-period pulse-like waveform, the conventional system may suffer from low-frequency resonance that will cause a considerable amplification of the isolator displacement and endanger the isolated structure (Lu et. al., 2003; Makris and Chang, 2000). In order to overcome this problem, some researchers have investigated the possibility of using active isolation systems, which combines the isolation system with an active device (Riley et. al., 1998), which provides an active control force to the isolation system. Due to its adaptive nature, an active isolation system is generally able to considerably improve the seismic performance of the isolation system subjected to earthquakes with either near-fault or far-field characteristics, provided that a proper control law is employed and a large amount of control energy is provided. However, an active control system usually requires a larger amount of control energy or control force. Especially when one considers that the structure to be isolated may have a very large mass. Because of this reason, the application of active isolation systems is hindered and limited. In addition, an active control system may also have control stability problem, if an improper control method is adopted or malfunction of the control system occurs.

From the above discussions, it is known that a conventional passive isolation system for equipment may perform well and are able to effectively reduce the response of equipments for earthquakes within the design range; however they may not also perform well, when subjected to an unusual or unpredicted earthquake that are outside or beyond the design range. Here, a usual earthquake means, for example, a pulse-like near-fault earthquake, or an earthquake with a very high intensity. Hence, in order to further protect valuable precision equipment from seismic attack, the development of an isolation system that has an adaptive nature and requires less control energy demand may be desirable.

Based on the above thought, the concept of semi-active isolation systems was proposed by researchers (Yang and Agrawal, 2002; Narasimhan and Nagarajaiah, 2005). A semi-active isolation system generally consists of a set of passive isolation bearings and a certain type of semi-active control devices, such as MR damper (Sahasrabudhe and Nagarajaiah, 2005), variable friction damper (Lu, 2004a; Lu et. al., 2004; Chen and Chen, 2004a; Chen and Chen, 2004b), or semi-active fluid damper (Symans and Constantinou, 1997), etc. A semi-active device is basically a “variable” passive device. The direction of the control force is always in opposite to the direction of the relative motion of the system. A semi-active device generally requires much less control energy, as compared with that of an active device. Since it is basically a passive device, it will not pump energy into the controlled structures. As a result, the effect of control spillover and control instability can be avoided.

This paper proposes a semi-active isolation system for the seismic protection of equipment. This isolation system, named “Piezoelectric Smart Isolation System (PSIS)”, is composed of a passive sliding isolation and a variable friction damper with an embedded piezoelectric actuator. The clamping force of the friction damper can be controlled by changing the input voltage of the piezoelectric actuator, which has the features of low energy demand and quick response. Due to the static friction of the sliding isolation, motion of the PSIS will not be activated nor amplified by a low-amplitude excitation, such as ambient vibration. When the PSIS is activated by an earthquake above a threshold level, the slip force of the piezoelectric friction damper, which provides a resistant and energy dissipating force to the system, can be regulated on-line by a controller for suppressing the response of the isolated equipment. Through a numerical simulation, the seismic performance of the PSIS will be investigated in this paper. The piezoelectric coefficient, which describes the relation between the clamping force and the control voltage of the damper, will be obtained from a piezoelectric actuator test, and then used in the simulation.

PIEZOELECTRIC SMART ISOLATION SYSTEM (PSIS)

Fig. 1 shows the schematic diagram of a piezoelectric smart isolation system, which consists of a set of sliding isolators and a piezoelectric friction damper (PFD). The isolators themselves have resilient ability. If the friction damper is removed, the system becomes a conventional “passive” isolation system.

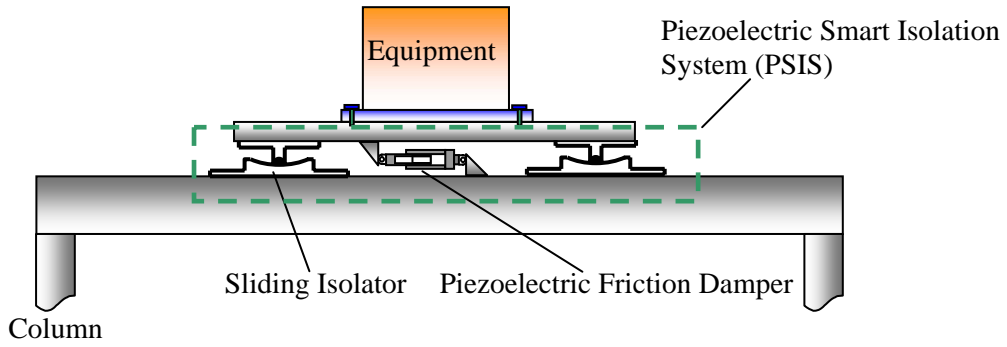


Figure 1. Schematic diagram of a piezoelectric smart isolation system.

Fig. 2 shows the schematic diagram of the piezoelectric friction damper for the PSIS. A piezoelectric actuator is embedded in the PFD to provide a controllable clamping force for the damper.

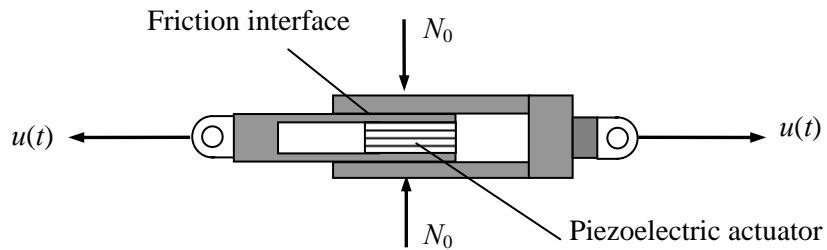


Figure 2. Schematic diagram of a piezoelectric friction damper (PFD).

Fig. 3 shows the block diagram for the control of a PFD. As shown in the figure, in order to drive the piezoelectric actuator in a desired way, a voltage amplifier and a controller are needed. The controller can be a digital controller that usually consists of a micro-computer with an analog/digital control card. The voltage amplifier is used to provide the piezoelectric actuator a controllable driving voltage. The features of the piezoelectric actuator and the voltage amplifier will be explained more detail in the following sub-sections.

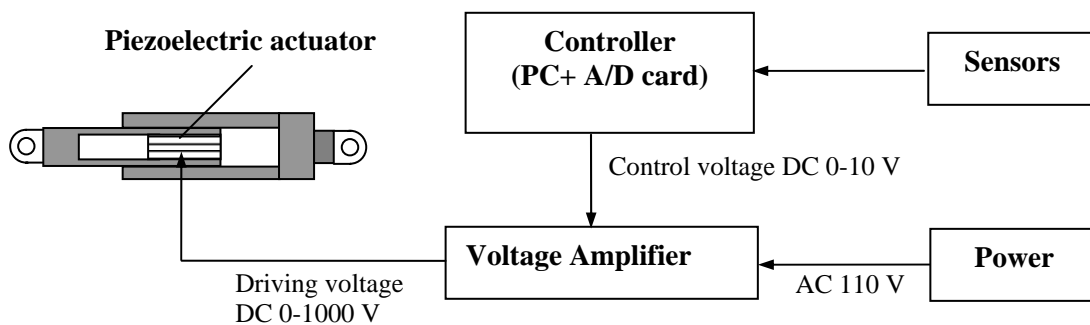


Figure 3. Block diagram for the control of a piezoelectric friction damper.

As shown in Fig. 2, the piezoelectric actuator in the damper is initially compressed by a pre-load N_0 , in order to obtain a better performance. With this pre-load, the clamping force applied on the friction interface of the PFD should be determined by the following equation

$$N(t) = N_0 + C_z V(t) \quad (1)$$

where $N(t)$ represents the controllable clamping force, $V(t)$ is the driving voltage of the piezoelectric actuator, C_z denotes the piezoelectric coefficient whose physical meaning is the force generated per volt. Based on Eq. (1), the damper force $u(t)$ of the PFD can be written as

$$u(t) \leq u_{\max}(t) = \mu_d N(t) \quad (2)$$

where $u_{\max}(t)$ and μ_d denote the slip force (maximum friction force) and the friction coefficient of the PFD, respectively. From Eq.(1) and (2), it is evident that by controlling the driving voltage $V(t)$, the clamping force $N(t)$ as well as the slip force $u_{\max}(t)$ of the PFD can be varied in a desirable way. Moreover, the piezoelectric coefficient C_z can be treated as a measurement of the efficiency of the piezoelectric actuator, since a larger C_z implies that a higher pushing force can be generated by the actuator with a lower voltage. The piezoelectric coefficient will be explained more detail in the next section.

Table 1. Specifications of the piezoelectric actuator.

Manufactory	Piezomechanik GmbH (Germany)
Modal Number	HPSst 1000/25-15/40
Dimensions(mm)	$\phi 35 \times \phi 14 \times 63$
Max Stroke(μm)	55
Input Voltage(v)	-200~1000
No. of Layers(n)	68
$d_{33}(\text{m/v})$	500×10^{-12}
$Y_{33}^E(\text{N/m}^2)$	6×10^{10}
Stiffness($\text{N}/\mu\text{m}$)	300
Resonance Frequency(kHz)	25
Max. Force Generation(N)	13000
Max. Compr. Load(N)	22000



Figure 4. Piezoelectric actuator.

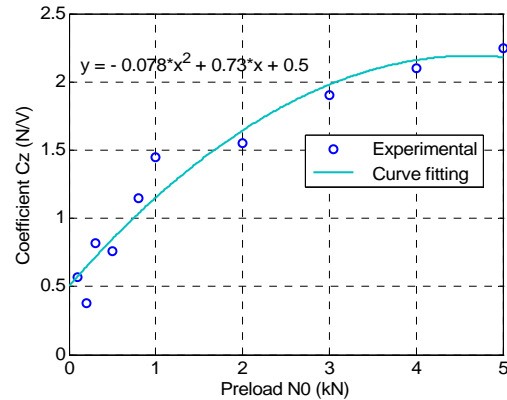


Figure 5. Relation of coefficient C_z vs. preload N_0 .

Piezoelectric Actuator in the PFD

As mentioned previously, the clamping force $N(t)$ of the PFD will be regulated by an embedded piezoelectric actuator. Fig. 4 shows the photo of a typical commercial piezoelectric actuator which can be purchased from the market. Table 1 lists the specifications of the piezoelectric actuator shown in Fig. 4. The length of a piezoelectric actuator can be elongated by a driving voltage. In a free-end (unloaded) condition, the elongation of the piezoelectric actuator is approximately proportional to the

input voltage. In order to generate a pushing force, the piezoelectric actuator must be properly restrained at its two ends. The condition of the restraints and the stiffness of the boundaries at the two ends of the actuator will affect the force generated. At a given input driving voltage, stiffer boundaries will generate a higher pushing force. The magnitude of the force generated is proportional to the piezoelectric coefficient C_z , which is defined as the force generated by the actuator per volt. Furthermore, in addition to the stiffness of the boundary, the coefficient C_z also depends on the initial compression force N_0 preloaded on the piezoelectric actuator. Fig. 5 shows the relation curve between the preload N_0 and the piezoelectric coefficient C_z of the piezoelectric actuator shown in Fig. 4. These data were obtained by a piezoelectric actuator test. In the test N_0 was varied from 0 to 5 kN. Since a value of C_z is affected by several factors, a test on the piezoelectric actuator is generally required to determine the actual C_z . The experimental result in Fig. 5 shows that the relation between C_z and N_0 is not linear, rather it is closer quadratic function.

Voltage Amplifier

A piezoelectric actuator requires a driving DC power with a high voltage up to 1000 volt. More importantly, the voltage of the driving power must be controllable. On the other hand, the control voltage provided by a controller such as the one shown in Fig. 3 (a PC with an A/D control card) is usually has a range of $\pm 10V$ DC only. This power is generally not sufficient to drive the piezoelectric actuator. Therefore, a voltage amplifier may be needed to amplify the control voltage of the controller and to provide the PFD the desired driving voltage. Fig.6 shows the outlook of the voltage amplifier used in this study. Table 2 lists the specification data of this amplifier. As shown in the table, the amplifier has a DC voltage gain of 100V/V, so it is able to amplify a 0-10V DC voltage to a range of 0-1000V DC. In addition, the maximum output electric current of the amplifier is merely 10 mA.

Table 2. Specifications of the voltage amplifier.

Manufactory	TREK, Inc. (USA)
Modal Number	601C-1-L-CE-EX
Output Voltage Range	0~+1000 V DC
Output Current Ranges	0~ ± 10 mA DC
Input Voltage Range	0~+10V DC
Input Impedance	25K Ω
DC Voltage Gain	100V/V
DC Voltage Gain Accuracy	Better than 0.1% of full scale
Large Signal Bandwidth	DC to greater than 8kHz (1% distortion)



Figure 6. Voltage amplifier.

Since the output power of the voltage amplifier is equal to the input power of the piezoelectric actuator, the power demand of the actuator can be computed by the following equation

$$P(t) = V(t)I(t) \quad (3)$$

where $P(t)$ and $I(t)$ are the electric power and current provided by the amplifier, respectively. Moreover, the accumulative energy consumed by the actuator can be computed by

$$E(t) = \int_0^t P(\tau)d\tau \quad (4)$$

where $E(t)$ denotes the accumulative consumption of the control energy of the actuator. Because the demand on the electric current $I(t)$ for a piezoelectric actuator is generally very low, from Eq.(2) and

(3) the control energy required by a piezoelectric actuator will be small, even though the driving voltage of the actuator is relatively higher.

SEMI-ACTIVE CONTROL LAW FOR PSIS

The proposed PSIS needs an on-line control law to decide the clamping force of the PFD. A control law named Semi-active Modal Control proposed by Lu (2004b) was adopted in this study. This semi-active control law was modified based on an active modal control law. In a modal control method, the motion of a controlled system is reshaped by merely controlling some selected vibration modes. The control force determined by an active modal control method can be written in a general form

$$\hat{u}(t) = \hat{\mathbf{G}} \mathbf{y}(t) \quad (5)$$

where $\hat{u}(t)$ represents the control target force, $\mathbf{y}(t)$ denotes the sensor measurement, $\hat{\mathbf{G}}$ is the constant feedback gain that is a function of the target modal values of the selected controlled modes. For a given set of target modal values, Lu (2004b) have derived a matrix formula that can systematically generate the gain $\hat{\mathbf{G}}$. This formula was adopted in this study.

Furthermore, the control force determined by Eq. (5) can not be directly applied to the PFD, because the PFD damper is basically a variable passive damper that can only provide a control force whose direction is opposite to the direction of the slip velocity or to the direction of the tendency to slip. In other words, the control force $\hat{u}(t)$ determined by Eq. (5) may not be completely achievable. Due to this reason, the above modal control method must be modified, in order to suit the property of the PFD. The clamping force of the PFD determined by the semi-active control law proposed by Lu (2004b) may be written as

$$N(t) = H(u(t) \hat{u}(t)) \frac{|\hat{u}(t)|}{\mu_d} \quad (6)$$

where $H(u(t) \hat{u}(t))$ represents a Heaviside function which is defined as

$$H(u(t) \hat{u}(t)) = \begin{cases} 1 & \text{for } u(t) \hat{u}(t) \geq 0 \\ 0 & \text{for } u(t) \hat{u}(t) < 0 \end{cases} \quad (7)$$

Once the desired clamping force is determined from Eq. (6), the desired driving voltage for the piezoelectric actuator can be derived from Eq. (1) and expressed in the following form

$$V(t) = \frac{(N(t) - N_0)}{C_z} \quad (8)$$

In practice, the value of $V(t)$ should also be limited by the voltage amplifier and the piezoelectric actuator used, so the following constraint should be imposed

$$0 \leq V(t) \leq V_{\max} \quad (9)$$

where V_{\max} denotes the upper bound of $V(t)$, which is equal to 1000 V if the actuator and the amplifier shown in Table 1 and Table 2, respectively, are used. By using Eq. (9) in Eq. (1), we obtain a lower and an upper bounds for both the clamping force $N(t)$ and the slip force $u_{\max}(t)$ of the PFD i.e.,

$$N_0 \leq N(t) \leq N_{\max} \quad (10)$$

$$\mu_d N_0 \leq u_{\max}(t) \leq \mu_d N_{\max} \quad (11)$$

where

$$N_{\max} = N_0 + C_z V_{\max} \quad (12)$$

EVALUATION ON SEISMIC PERFORMANCE OF PSIS

Parameters of numerical model

In order to demonstrate the seismic isolation effectiveness of the PSIS system, the seismic performance of the structure-equipment model shown in Fig. 7 has been studied numerically in this section. The equipment is isolated by the PSIS and controlled by the proposed semi-active modal control law. The control goal was set to increase the modal damping ratios of the first mode to 30%, and at the same time to keep the modal frequency and the mode shape unchanged. The symbols x_e and x_s in Fig. 7 denote the relative-to-ground displacements of the equipment and the structure, respectively. All other notations shown in the figure are defined in Table 3. The performance of the PSIS will be compared with those of a passive and an active isolation system. The passive isolation can be treated equivalently as the uncontrolled case of the PSIS. Table 3 lists the numerical values of the parameters of the structure-equipment model used in the numerical simulation. In addition, the specification data shown in Table 1 and 2 for the piezoelectric actuator and the voltage amplifier were also adopted in the simulation.

As shown in Table 3, the preload N_0 of the piezoelectric actuator was taken to be 1 kN in the simulation, therefore according to Fig. 4 the corresponding piezoelectric coefficient C_z should be 1.45 N/V. This value of C_z was taken in the simulation. The natural frequency of the isolation system is 0.4 Hz; while, the frequency of the primary structure is 5 Hz. The mass ratio of the equipment and structure is 1/10000, so the interaction between equipment and structure is almost negligible. The friction coefficients of the isolators and the PFD were taken to be 0.03 and 0.2, respectively. In all simulation, the time interval for the numerical analysis was taken to be 0.005 second. Moreover, in order to quantify the isolation effectiveness of the isolation systems, in the following discussions, two system responses, i.e., the isolator displacement and the equipment acceleration are chosen as the performance indices to be compared. The purpose of the PSIS is to reduce both responses.

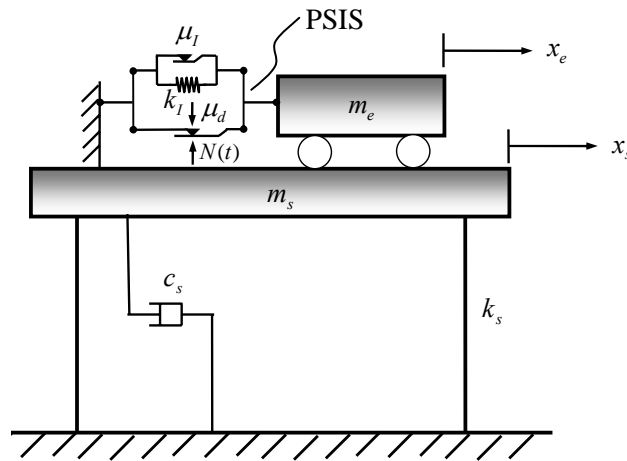


Figure 7. Mathematic model of the structure-equipment model with the PSIS.

The ground acceleration record obtained in the 1979 Imperial Valley earthquake (El Centro Array #6 station) (Naeim, and Kelly, 1999) will be used as the input ground motions in the simulation. The acceleration waveform of this record is depicted in Fig. 8. The record can be classified as a near-fault earthquake, since a long-period pulse can be clearly observed in the waveform of this near-fault earthquake, as shown in Fig. 8.

Table 3. Parameters of the structure-equipment model with the PSIS.

	Parameter	Value
Primary structure	Structure mass (m_s)	10000 ton
	Structure stiffness (k_s)	9.8696×10^6 kN/m
	Damping coefficient (c_s)	3.141×10^4 kN-sec/m
	Natural frequency (ω_s)	5 Hz
	Damping ratio (ζ_s)	5 %
Equipment and PSIS	Equipment mass (m_e)	1 ton
	Preload of PFD (N_0)	1 kN
	piezoelectric coefficient (C_z)	1.45 N/V
	Friction coeff. of isolator (μ_I)	0.03
	Friction coeff. of damper (μ_d)	0.2
	Isolation frequency (ω_I)	0.4 Hz
	Base isolation stiffness (k_I)	17.546 kN/m

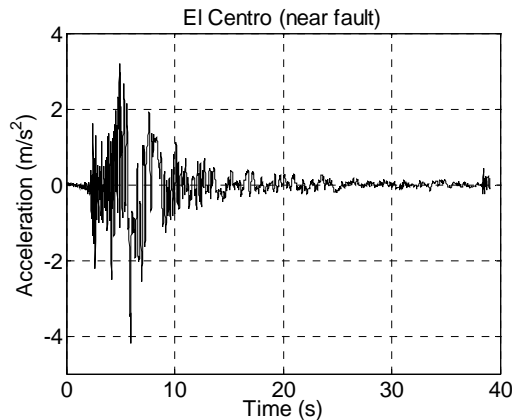
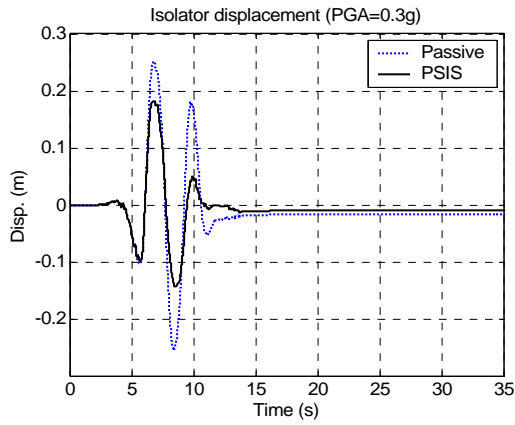


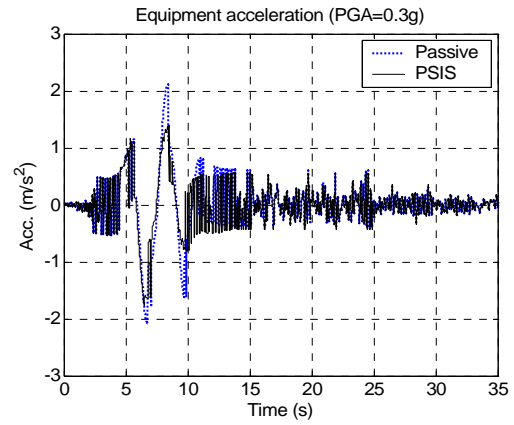
Figure 8. Near-fault ground acceleration record for simulation.

Comparison of the PSIS and a passive isolation system

Fig. 9 compares the time history responses of the PSIS and a passive isolation system, when they are subjected to the near-field earthquake. Note that in the figure the PGA (peak ground acceleration) of the earthquake has been scaled to 0.3g for the purpose of comparison. Figure 9 shows that due to the pulse excitation existing in the near-fault earthquake, both isolation systems exhibit an obvious long-period pulse-like oscillation behavior in both acceleration and displacement responses. However, Fig. 9 also shows that the PSIS is able to reduce the maximum equipment acceleration and the maximum isolator displacement simultaneously, as compared with the passive isolation. This implies that the PSIS is able to effectively suppress the base displacement enlarged by the pulse waveform of the near-fault earthquake, without scarifying the response of the structural acceleration. This behavior is usually difficult to be achieved by using a passive isolation system. On the other hand, Fig. 10 shows the simulated results of the piezoelectric driving voltage and the clamping force of the PFD during the earthquake. As shown in Fig. 10(a), the driving voltage is bounded by $0 \leq V(t) \leq 1000V$. As a result, from Eq.(12) the clamping force is bounded by $0 \leq N(t) \leq 2.450kN$ as shown in Fig. 10(b), with the given numerical values of the parameters mentioned in Tables 1-3.

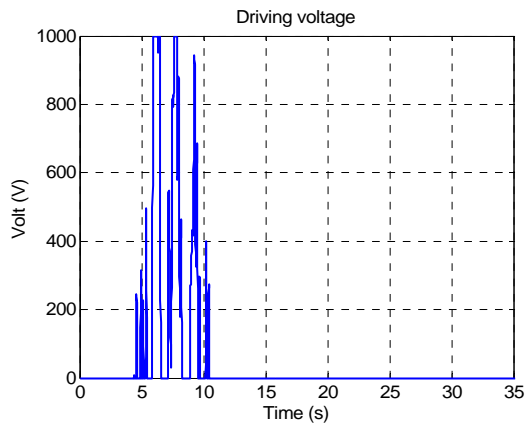


(a) Isolator displacement.

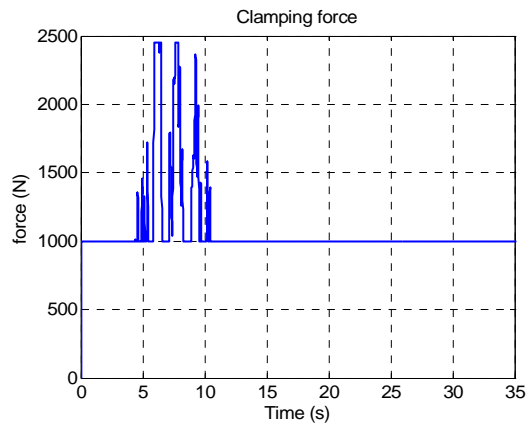


(b) Equipment acceleration.

Figure 9. Comparison of system response of passive isolation and PSIS (PGA=0.3g).



(a) Control voltage



(b) Clamping Force

Figure 10. Control voltage and clamping force of PSIS (PGA=0.3g)

For the concern of control energy, Fig. 11 compares the energy dissipated by the PFD and the accumulation of control energy $E(t)$ of the PFD, which is calculated by using Eq. (4). Note that to be conservative, in this study, a maximum supply current $I = 10\text{mA}$ of the amplifier was used. On the other hand, the energy dissipated is obtained by integrating the product of the friction force and the slip displacement of the PFD. From Fig. 11 it is evident that the control energy demand is much lower than the energy dissipated.

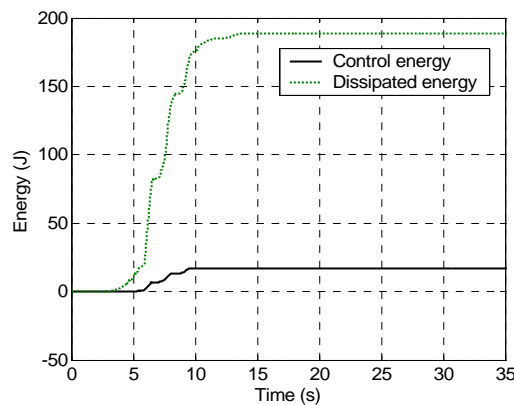


Figure 11. Comparison of energy (PGA=0.3g).

Comparison of the PSIS and an active isolation system

Fig. 12 compares the time history responses of the PSIS and an active isolation system, when they are subjected to the near-fault earthquakes. Here, the active isolation system means a sliding isolation system equipped with an active device, which is able to produce an active force to the isolation system. From the diagram, it is observed that the PSIS is able to closely follow the responses of the active system in the near-fault earthquake, even though the maximum responses values of the PSIS is slightly higher than those of the active system.

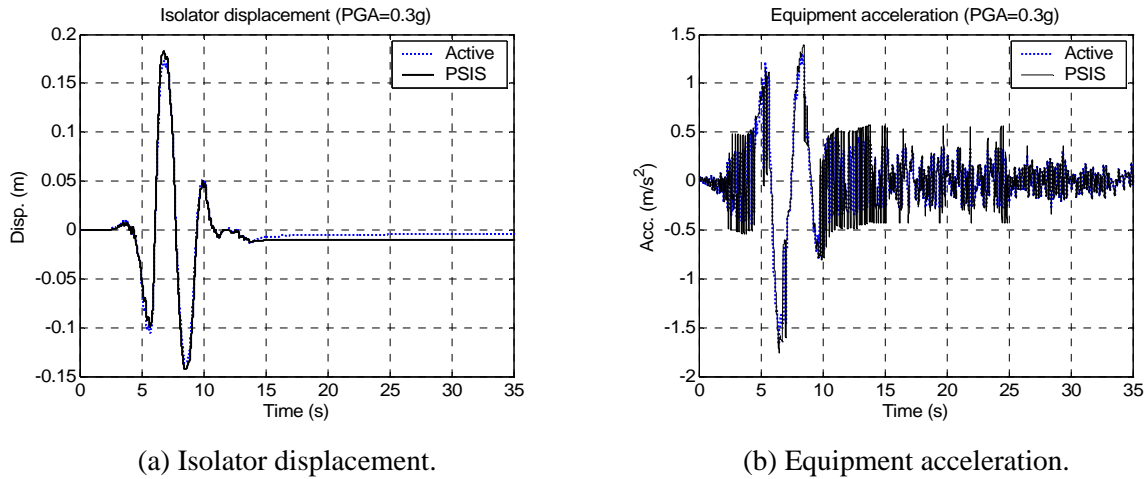


Figure 12. Comparison of system responses of active isolation and PSIS (PGA=0.3g).

Fig. 13 compares the hysteresis loop of the PFD damper in the PSIS and the loop that of the active device in the active isolation system. As shown, the hysteresis loop of the PFD is similar to that of the active device, except that the damper force $u(t)$ of the PDF is bounded by an upper and a lower bound. The lower bound is due to the preload N_0 while the upper bound is due to the maximum control voltage V_{\max} . These lower and upper bounds of $u(t)$ can be calculated by Eq. (11). With the simulated parameters, these bounds are: $200\text{N} \leq u(t) \leq 490\text{N}$. Due to the similarity of the hysteresis loops, the amount of the energy dissipated by the PDF is close to that of the active device. This explains the reason why the responses of the PSIS and the active isolation shown in Fig. 12 are so close.

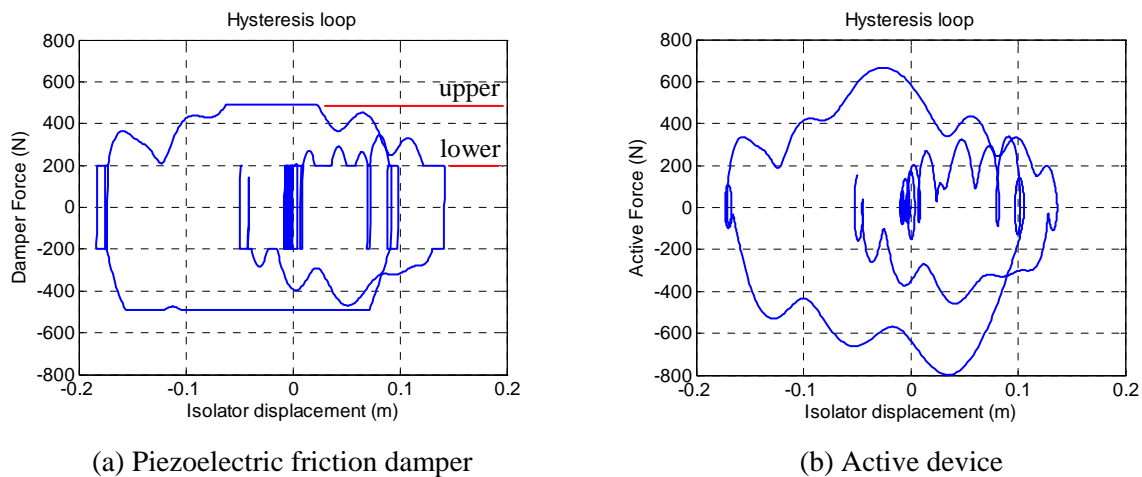


Figure 13. Comparison of hysteresis loops of the PFD damper and the active device (PGA=0.3g).

Fig. 14 compares the accumulative control energy demands of the PFD and the active isolation system. The control energy of the active isolation is obtained by integrating the product of the actuator force and the isolator displacement. As shown in the figure, the control energy demand of the PSIS is far

below that of the active isolation. The control energy of the active isolation is about ten times of the PSIS.

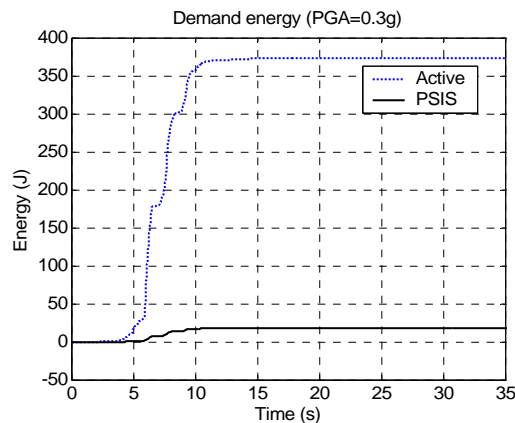


Figure 14. Comparison of control energy of the PSIS and the active isolation (PGA=0.3g).

CONCLUSIONS

In order to enhance seismic resistance ability of precision equipments, this paper proposed an equipment isolation system, named “Piezoelectric Smart Isolation System (PSIS)”. This system is mainly composed of a sliding isolation system and a piezoelectric friction damper (PFD). In response to the motion of the PSIS, the clamping force as well as the slip load of the PFD can be controlled on line by an embedded piezoelectric actuator. The piezoelectric actuator is powered and controlled through a voltage amplifier. Because the electric current required by the piezoelectric actuator is very small, the energy demand for the control of the PSIS is very low. By using the experimental data obtained from the test of a piezoelectric actuator, the seismic performance of the PSIS was evaluated numerically and compared with those of a passive and an active isolation system. The numerical results demonstrated that the performance of the proposed PSIS system is superior to the passive isolation system in reducing both the equipment acceleration and isolator displacement when subjected to a near-fault earthquake with a long-period pulse waveform. Furthermore, when compared with the active isolation system, the PSIS system is able to closely follow the responses of the active system. The consumption of the control energy required by the PSIS is only about ten percents of that of the active system.

ACKNOWLEDGMENTS

This research was supported in part by National Science Council of R.O.C. (Taiwan), through Grant 95-2625-Z-327-001. This support is gratefully acknowledged.

REFERENCES

- Chen, C. and G. Chen (2004) "Shake table tests of a quarter-scale three-storey building model with piezoelectric friction dampers", *Structural Control and Health Monitoring*, 11, 239–257.
- Chen, G. and C. Chen (2004) "Semiactive control of the 20-Story benchmark building with piezoelectric friction dampers", *Journal of Engineering Mechanics*, 130(4), 393–400.
- Loh, C. H. (1999) "Interpretation of structural damage in 921 Chi-Chi-earthquake" *Proceedings of International Workshop on Chi-Chi, Taiwan Earthquake of September 21*, Dec. 14-17, 5-1 ~ 5-77.
- Lu, L. Y. and Y. B. Yang (1997) "Dynamic Response of Equipment in Structures with Sliding Support," *Earthquake Engineering and Structural Dynamics*, 26(1), 61-76.

- Lu, L. Y., M. H. Shih, S. W. Tzeng and C. S. Chang Chien (2003) "Experiment of a sliding isolated structure subjected to near-fault ground motion" *Proceedings of the 7th Pacific Conference on Earthquake Engineering*, February 13-15, Christchurch, New Zealand.
- Lu, L. Y. (2004a) "Predictive control of seismic structures with semi-active friction dampers" *Earthquake Engineering and Structural Dynamics*, **33**(5), 647-668.
- Lu, L. Y. (2004b) "Semi-active modal control for seismic structures with variable friction dampers" *Engineering Structures*, **26**(4), 437-454.
- Lu, L. Y., L. L. Chung, G. L. Lin, (2004) "A general method for semi-active feedback control of variable friction dampers" *Journal of Intelligent Material Systems and Structures*, **15**(5), 393-412.
- Makris, N. and S. P. Chang (2000) "Effect of viscous, visoplastic and friction damping on the response of seismic isolated structures" *Earthquake Engineering and Structural Dynamics*, **29**, 85-107.
- Meirovitch, L. (1990) *Dynamics and Control of Structures*, John Wiley & Sons:New York.
- Naeim, F. and J. M. Kelly (1999) *Design of Seismic Isolated Structures*, Chapter 4, John Wiley & Sons, Inc., New York.
- Narasimhan, S. and S. Nagarajaiah (2005) "A STFT semiactive controller for base isolated buildings with variable stiffness isolation systems," *Engineering Structures*, **27**, 514-523.
- Riley, M. A. and A. M. Reinhorn, and S. Nagarajaiah, (1998) "Implementation issues and testing of a hybrid sliding isolation system", *Engineering Structures*, **20**(3), 144-154.
- Sahasrabudhe, S. S. and S. Nagarajaiah, (2005) "Semi-active control of sliding isolated bridges using MR dampers: an experimental and numerical study" *Earthquake Engineering and Structural Dynamics*, **34**, 965-983.
- Symans, M. D and M. C. Constantinou (1997) "Seismic testing of a building structure with a semi-active fluid damper control system" *Earthquake Engineering and Structural Dynamics*, **26**, 759-777.
- Ungar, E. E. and D. H. Sturz, and C. H. Amick, (1990) "Vibration Control design of high technology factories", *Sound and Vibration*, 20-27.
- Yang, J. N. and A. K. Agrawal (2002) "Semi-active hybrid control systems for nonlinear building against near-fault earthquakes, " *Engineering Structures*, **24**(3), 271-280.
- Yang, Y. B., L. Y. Lu and J. D. Yau (2005) "Chapter 22: *Structure and Equipment Isolation*" *Vibration and Shock Handbook*, edited by C. W. de Silva, CRC Press, Taylor & Francis Group.